Polymer Journal, Vol. 37, No. 12, pp. 913–924 (2005)

Wormlike Micelles of Polyoxyethylene Dodecyl $C_{12}E_j$ and Heptaoxyethylene Alkyl C_iE_7 Ethers. Hydrophobic and Hydrophilic Chain Length Dependence of the Micellar Characteristics

Satoko SHIRAI and Yoshiyuki EINAGA†

Department of Chemistry, Nara Women's University, Kitauoyanishi-machi, Nara 630-8506, Japan

(Received July 22, 2005; Accepted August 15, 2005; Published December 15, 2005)

ABSTRACT: The micelles formed with pentaoxyethylene $C_{12}E_5$ and heptaoxyethylene $C_{12}E_7$ dodecyl ethers and heptaoxyethylene tetradecyl ether $C_{14}E_7$ in dilute aqueous solutions were characterized by static (SLS) and dynamic light scattering (DLS) experiments at several temperatures T below the critical points. The SLS results were successfully analyzed by using a thermodynamic theory formulated with wormlike spherocylinder model for SLS of micelle solutions, thereby yielding the molar mass M_w of the micelles as a function of c along with the cross-sectional diameter d. The radius of gyration $\langle S^2\rangle^{1/2}$ and the hydrodynamic radius R_H of the micelles as functions of M_w were found to be also well described by the corresponding theories for the wormlike spherocylinder or wormlike chain models. Combining the present and previous results for various C_iE_j (polyoxyethylene alkyl ether) micelles, effects of the hydrophobic (alkyl) i and hydrophilic (oxyethylene) chain length j on the micellar characteristics have been clarified as: (i) The micellar length L becomes larger for larger i and smaller j. (ii) The d values do not significantly vary with the values of i and j. (iii) The stiffness parameter λ^{-1} decreases with increasing i at fixed j and increases with increasing j at fixed i. (iv) The spacing s between adjacent oxyethylene tails of the surfactant molecule on the micellar surface gradually increases with increasing i and j. [DOI 10.1295/polymj.37.913]

KEY WORDS Light Scattering / Radius of Gyration / Diffusion Coefficient / Hydrodynamic Radius / Polyoxyethylene Alkyl Ether / Wormlike Micelle /

In this series of experimental work on the wormlike micelles of polyoxyethylene alkyl ethers $H(CH_2)_i(OCH_2CH_2)_jOH$ (abbreviated C_iE_j),[1–4] we have investigated micelle characteristics such as the weight-average molar mass M_w, mean-square radius of gyration $\langle S^2\rangle$, and hydrodynamic radius R_H as functions of surfactant mass concentration c by static (SLS) and dynamic light scattering (DLS) measurements. We have determined the values of $M_w(c)$ at a specified c along with the cross-sectional diameter d of the micelles from the analysis of the SLS data by using a molecular thermodynamic theory[5,6] formulated with the wormlike spherocylinder model. It is then found that molar mass M_w dependence of $\langle S^2\rangle$ and R_H is quantitatively represented by the chain statistical[7] and hydrodynamic[8–10] theories based on the wormlike chain and spherocylinder models, respectively, thereby yielding the values of the stiffness parameter λ^{-1}. These analyses have demonstrated that the C_iE_j micelles assume a shape of flexible cylinder. We have so far characterized micelles of the surfactants $C_{10}E_5$, $C_{10}E_6$, $C_{12}E_6$, $C_{14}E_6$, $C_{16}E_7$, $C_{18}E_7$, $C_{14}E_8$, $C_{16}E_8$, and $C_{18}E_8$, and examined effects of the hydrophobic i and hydrophilic chain length j on size, structure, and flexibility of the micelles.

Solution properties of the C_iE_j micelles have been the subject of considerable research.[11–24] Brown and his coworkers[11–13] studied solution properties of $C_{12}E_5$, $C_{12}E_6$, $C_{12}E_7$, and $C_{12}E_8$ micelles by SLS, DLS, and pulsed field gradient NMR measurements. Similar studies were performed for $C_{12}E_5$, $C_{12}E_6$, and $C_{12}E_8$ micellar solutions by Kato *et al.*[16,17] They showed that the C_iE_j micelles grew in size with raising temperature and increasing surfactant concentration, and that intermicellar thermodynamic and hydrodynamic interactions strongly increase with concentration. Bernheim-Groswasser *et al.*[24] realized by cryo-TEM observations that in the growth of the $C_{12}E_5$ micelles thread-like or polymer-like micelles were evolved in the solutions examined, especially to the greater length in the vicinity of the lower consolute point.

Although the solution properties of micelles are analogous to those of polymer solutions, the micelles possess the essential difference from polymers that the micellar size or length is not chemically fixed but, in general, depends on surfactant concentration. For this reason, analyses of the scattering data for micelle solutions encounter difficulties in the performance for separate determination of concentration-dependent micellar growth and intermicellar interactions. In order to circumvent this problem, we have utilized the molecular thermodynamic theory[5,6] for unequivo-

†To whom correspondence should be addressed (E-mail: einaga@cc.nara-wu.ac.jp).

cal determination of M_w of the micelles from the analysis of the SLS results in our previous studies.[1–4]

In the present study, we have extended our previous work[1–4] to the micelle solutions of the surfactants $C_{12}E_5$, $C_{12}E_7$, and $C_{14}E_7$. The main aim is to examine the effects of the hydrophobic and hydrophilic chain lengths on the micellar characteristics such as length, cross-sectional diameter, stiffness, and structure, in combination with the previous data for other C_iE_j micelles.

EXPERIMENTAL SECTION

Materials

The surfactant $C_{12}E_5$, $C_{12}E_7$, and $C_{14}E_7$ samples were purchased from Nikko Chemicals Co. Ltd. and used without further purification. The solvent water used was high purity (ultrapure) water prepared with Simpli Lab water purification system of Millipore Co.

Phase Diagram

Cloud-point temperature of a given solution was determined as the temperatures at which the intensity of the laser light transmitted through the solution abruptly decreased when temperature was gradually raised. The binodal for a given $C_{12}E_5$ micelle solution was determined by measuring the volume ratio of the two coexisting phases with the aid of the lever rule, where the concentration of the dilute phase was assumed to be substantially zero.

Static Light Scattering

SLS measurements were performed to obtain the weight-average molar mass M_w of the $C_{12}E_5$, $C_{12}E_7$, and $C_{14}E_7$ micelles. The scattering intensities were measured for each solution and for the solvent water at scattering angles θ ranging from 30 to 150° and at temperatures T ranging from 15.0 to 30.0 °C for $C_{12}E_5$ solutions, from 45.0 to 60.0 °C for $C_{12}E_7$ solutions, and from 25.0 to 55.0 °C for $C_{14}E_7$ solutions. The ratio $Kc/\Delta R_\theta$ was obtained for each solution as a function of θ and extrapolated to zero scattering angle to evaluate $Kc/\Delta R_0$. Here, c is the surfactant mass concentration, ΔR_θ is the excess Rayleigh ratio, and K is the optical constant defined as

$$K = \frac{4\pi^2 n^2 (\partial n/\partial c)_{T,p}^2}{N_A \lambda_0^4} \quad (1)$$

with N_A being the Avogadro's number, λ_0 the wavelength of the incident light in vacuum, n the refractive index of the solution, $(\partial n/\partial c)_{T,p}$ the refractive index increment, T the absolute temperature, and p the pressure. The plot of $Kc/\Delta R_\theta$ *vs.* $\sin^2(\theta/2)$ affords a good straight line for all the micelle solutions studied. From the slope of the straight line, we have determined the apparent mean-square radius of gyration $\langle S^2\rangle_{app}$ for the micelles at finite concentrations on the basis of the fundamental light scattering equation

$$\frac{Kc}{\Delta R_\theta} = \frac{1}{M_w(c)}\left(1 + \frac{1}{3}\langle S^2\rangle q^2\right) + 2A_2 c + \cdots \quad (2)$$

by using the $M_w(c)$ values determined as described below. Here, A_2 is the second virial coefficient and q is the magnitude of the scattering vector defined as

$$q = \frac{4\pi n}{\lambda_0}\sin(\theta/2) \quad (3)$$

The mean square radius of gyration $\langle S^2\rangle$ is denoted by $\langle S^2\rangle_{app}$, since it is possibly affected by intermicellar interactions at finite concentrations examined. We note that eq 2 corresponds to the equation derived for micelle solutions on the basis of the Ornstein–Zernike theory,[5] in which $\langle S^2\rangle$ in eq 2 is shown to be true z-average mean-square radius of gyration.

The apparatus used is an ALV DLS/SLS-5000/E light scattering photogoniometer and correlator system with vertically polarized incident light of 632.8 nm wavelength from a Uniphase Model 1145P He–Ne gas laser. For a calibration of the apparatus, the intensity of light scattered from pure benzene was measured at 25.0 °C at a scattering angle of 90°, where the Rayleigh ratio $R_{Uv}(90)$ of pure benzene for unpolarized scattered light with polarized incident light at a wavelength of 632.8 nm was taken as 11.84×10^{-6} cm^{-1}.[25,26]

The micellar solutions were prepared by dissolving appropriate amount of the surfactant in water. Complete mixing and micelle formation were achieved by stirring using a magnetic stirrer at least for one day. The solutions thus prepared were optically clarified by filtration through a membrane of 0.20 μm pore size and transferred into optically clean NMR tubes of 10 mm diameter which was used as scatterring cells. The weight concentrations w of test solutions were determined gravimetrically and converted to mass concentrations c by the use of the densities ρ of the solutions given below.

The refractive index increment $(\partial n/\partial c)_{T,p}$ was measured at 20.0, 25.0, and 30.0 °C for $C_{12}E_5$ solutions, at 45.0, 50.0, and 55.0 °C for $C_{12}E_7$ solutions, and at 30.0, 40.0, and 50.0 °C for $C_{14}E_7$ solutions, and at 632.8 nm with a Union Giken R601 differential refractometer. The results (in cm^3/g) are summarized as: for $C_{12}E_5$ solutions,

$$(\partial n/\partial c)_{T,p} = 0.1472 - 2.39 \times 10^{-4}(T - 273.15) \quad (4)$$

for $C_{12}E_7$ solutions,

$$(\partial n/\partial c)_{T,p} = 0.1269 \quad (5)$$

for $C_{14}E_7$ solutions,

$$(\partial n/\partial c)_{T,p} = 0.1342 - 1.93 \times 10^{-4}(T - 273.15) \quad (6)$$

Dynamic Light Scattering

DLS measurements were carried out to determine the translational diffusion coefficient D for the micelles in water at various temperatures in the one phase (L_1 phase) region below the phase separation boundary shown below by the use of the same apparatus and light source as used in the SLS studies described above. The normalized autocorrelation function $g^{(2)}(t)$ of scattered light intensity $I(t)$, *i.e.*,

$$g^{(2)}(t) = \frac{\langle I(0)I(t)\rangle}{\langle I(0)\rangle^2} \quad (7)$$

was measured at scattering angles θ ranging from 30 to 150°.

All the test solutions studied are the same as those used in the SLS studies. From the data for $g^{(2)}(t)$, we determined D by the equation

$$(1/2)\ln[g^{(2)}(t) - 1] = (1/2)\ln f - K_1 t + \cdots \quad (8)$$

$$D = \lim_{q\to 0} K_1/q^2 \quad (9)$$

Here, f is the coherence factor fixed by the optical system and K_1 is the first cumulant. It should be noted that the D values should be regarded as an average, since the micelles observed may have distribution in size.

The apparent hydrodynamic radius $R_{H,app}$ has been evaluated from the D values by[1,27,28]

$$D = \frac{(1 - vc)^2 M_w k_B T}{6\pi\eta_0 R_{H,app}} \left(\frac{Kc}{\Delta R_0}\right) \quad (10)$$

where v is the partial specific volume of the solute (micelle), k_B is the Boltzmann constant, and η_0 is the solvent viscosity.

Density

The solution density ρ required for the calculation of c and v was measured at 15.0 and 25.0 °C for $C_{12}E_5$ solutions, at 30.0 and 50.0 °C for $C_{12}E_7$ solutions, and at 30.0, 40.0, and 50.0 °C for $C_{14}E_7$ solutions with a pycnometer of the Lipkin-Davison type. For the former two micelle solutions, ρ has been found to be independent of surfactant weight fraction w at every temperature examined. Thus we have used the literature values of the density ρ_0 of pure water at corresponding temperatures for ρ, and the values of v of the micelles have been calculated as ρ_0^{-1}. For $C_{14}E_7$ solutions, ρ (in g/cm^3) and v (in cm^3/g) are summarized as:

$$\rho^{-1} = 0.99968 + 3.93 \times 10^{-4}(T - 273.15) + 1.878 \times 10^{-2} w \quad (11)$$

$$v = 1.01846 + 3.94 \times 10^{-4}(T - 273.15) \quad (12)$$

RESULTS

Phase Behavior

Figure 1 depicts the phase diagrams determined in the present work (unfilled symbols) for the aqueous solutions of $C_{12}E_5$, $C_{12}E_7$, and $C_{14}E_7$, along with the literature results (filled symbols) for those of $C_{12}E_5$, $C_{12}E_6$, and $C_{14}E_6$, where circles and triangles represent the cloud points and binodals, respectively. The large filled symbols for the $C_{12}E_6$ and $C_{14}E_6$ solutions are our previous results[1] and small filled circles for the $C_{12}E_5$ and $C_{12}E_6$ solutions denote the data reported by Bernheim-Groswasser *et al.*[24] and by Briganti *et al.*[29] It is seen that all the micelle solutions studied represent the phase separation behavior of the LCST (lower critical solution temperature) type and that the phase boundaries significantly shift to lower temperatures as the length of the hydrophobic chain in the surfactant molecules becomes longer at fixed hydrophilic chain length or as the hydrophilic chain length becomes shorter at fixed hydrophobic chain length. We can estimate the LCST temperatures for the $C_{12}E_7$, $C_{14}E_7$, $C_{12}E_6$, $C_{14}E_6$, and $C_{12}E_5$ micelle solutions as 65.5, 58.1, 51.7, 42.8, and 32.0 °C, respectively.

The phase behavior resembles the observations for real polymer solutions, in which the critical temperature T_c is shifted to lower values with increasing polymer molecular weight, when the phase diagram of the LCST type is observed. Thus, the results shown in Figure 1 suggest that the micellar size becomes larger as the alkyl chain of the surfactants becomes longer or the oxyethylene chain becomes shorter.

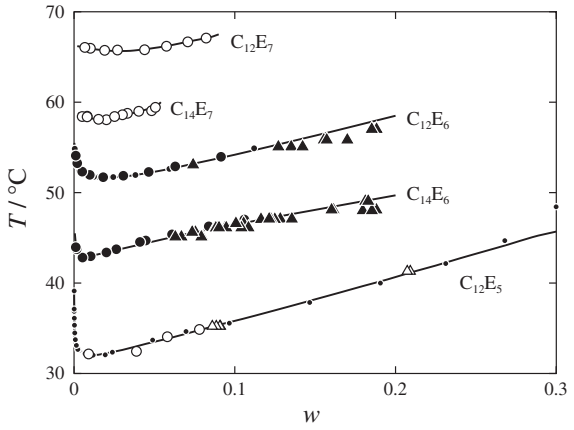

Figure 1. Phase diagrams of the micellar solutions of various C_iE_j molecules: circles, cloud points; triangles, binodals; unfilled symbols, present data; filled symbols, literature data.[1,24,29]

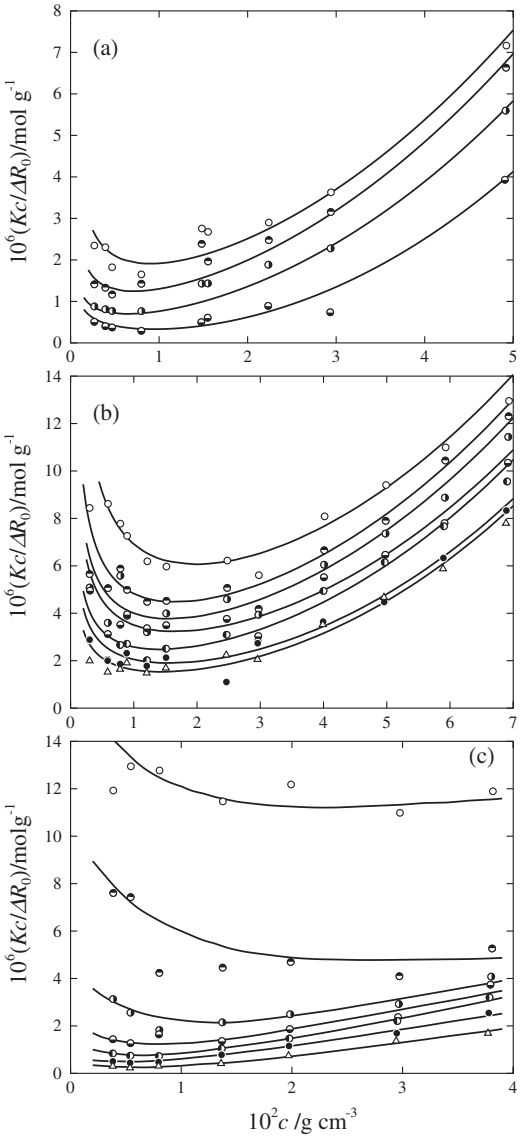

Figure 2. Plots of $(Kc/\Delta R_0)$ against c for the $C_{12}E_5$ (a), $C_{12}E_7$ (b), and $C_{14}E_7$ (c) micelle solutions at various T: (a) ○, 15.0 °C; ◓, 20.0 °C; ◑, 25.0 °C; ◒, 30.0 °C; (b) ○, 45.0 °C; ◓, 48.0 °C; ◑, 50.0 °C; ◒, 52.0 °C; ◐, 55.0 °C; ●, 58.0 °C; △, 60.0 °C; (c) ○, 25.0 °C; ◓, 30.0 °C; ◑, 35.0 °C; ◒, 40.0 °C; ◐, 45.0 °C; ●, 50.0 °C; △, 55.0 °C;

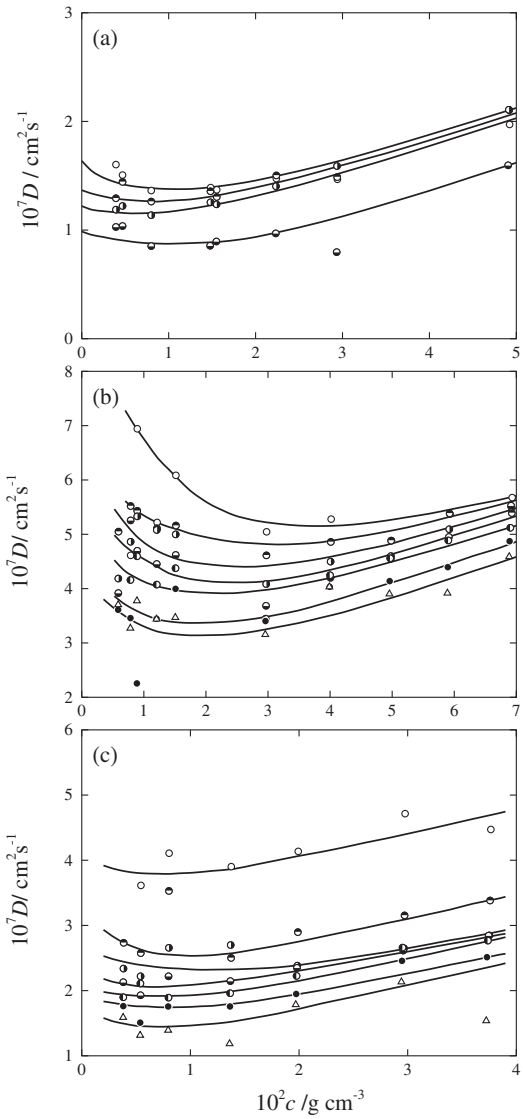

Figure 3. Plots of D against c for the $C_{12}E_5$ (a), $C_{12}E_7$ (b), and $C_{14}E_7$ (c) micelle solutions at various T: Symbols have the same meaning as those in Figure 2.

Light Scattering Results

In Figures 2a, 2b, and 2c, $Kc/\Delta R_0$ are plotted against c examined at various temperatures for all the solutions of the $C_{12}E_5$, $C_{12}E_7$, and $C_{14}E_7$ micelles, respectively. The data points at fixed T follow a curve convex downward and the $Kc/\Delta R_0$ value at fixed c decreases with increasing T.

Figures 3a, 3b, and 3c illustrate the plots of D against c determined from the $g^{(2)}(t)$ data by the cumulant method with eqs 8 and 9 for the $C_{12}E_5$, $C_{12}E_7$, and $C_{14}E_7$ micelles at various temperatures, respectively. It is found that the D value becomes smaller as T is raised, for any case of the micelle solutions.

DISCUSSION

Analysis of SLS Data

In order to determine the M_w values of the micelles at finite concentrations c, we have analyzed the present SLS data by employing a light-scattering theory for micellar solutions formulated by Sato[5,6] with wormlike spherocylinder model for polymer-like micelles as mentioned in the Introduction. In the theory, the micellar size or the aggregation number N of the surfactant molecules in the micelle and its distribution have been formulated on the basis of multiple equilibria among various micelles of different sizes and monomer, by representing chemical potentials of the micelles as functions of c in a similar fashion to the classical mean-field and recent molecular theoretical approaches.[30–32] The intermicellar thermodynamic

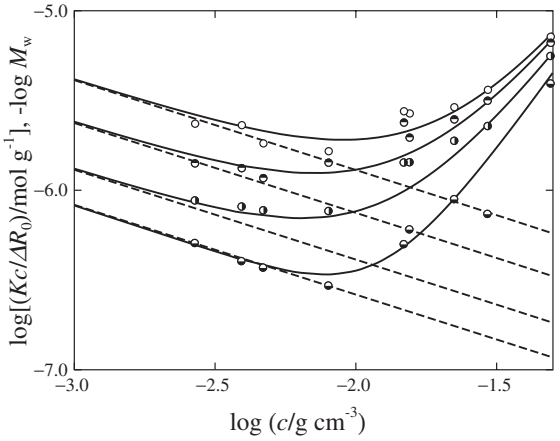

Figure 4. The results of the curve fitting for the plots of $Kc/\Delta R_0$ against c for the $C_{12}E_5$ micelle solutions at various T: Symbols have the same meaning as those in Figure 2a. The solid and dashed curves represent the calculated values of $Kc/\Delta R_0$ and $1/M_w(c)$, respectively. Temperatures T are 15.0, 20.0, 25.0, and 30.0 °C from top to bottom, respectively.

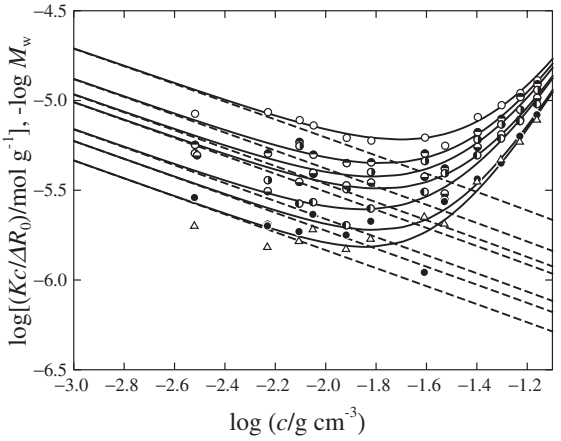

Figure 5. The results of the curve fitting for the plots of $Kc/\Delta R_0$ against c for the $C_{12}E_7$ micelle solutions at various T: Symbols have the same meaning as those in Figure 2b. The solid and dashed curves represent the calculated values of $Kc/\Delta R_0$ and $1/M_w(c)$, respectively. Temperatures T are 45.0, 48.0, 50.0, 52.0, 55.0, 58.0, and 60.0 °C from top to bottom, respectively.

interactions have been taken into account in the chemical potential on the basis of a statistical thermodynamic theory for stiff polymer solutions with the wormlike spherocylinder model.[6] Here, the model consists of a wormlike cylinder of contour length $L - d$ with cross-sectional diameter d and two hemispheres of diameter d which cap both ends of the cylinder, and stiffness of the wormlike cylinder is represented by the stiffness parameter λ^{-1}. It may represent a variety of the shape of polymer-like micelles, including a sphere, rigid rod, flexible and/or random-coil rod (or cylinder).

According to the general fluctuation theory,[33] the excess zero-angle Rayleigh ratio ΔR_0 is formulated from the chemical potentials of the solute micelles. The result for $Kc/\Delta R_0$ reads

$$\frac{Kc}{\Delta R_0} = \frac{1}{M_w(c)} + 2A(c)c \qquad (13)$$

where $M_w(c)$ is the weight-average molar mass of the micelles and $A(c)$ is the apparent second virial coefficient in a sense that it is comprised of the second, third, and the higher virial coefficient terms. Both are functions of c, containing three parameters d, free-energy parameter g_2, and strength $\hat{\varepsilon}$ of the attractive interaction between spherocylinders. In these, g_2 represents the difference in Gibbs free energy between surfactant molecules located in the end-capped portion to those in the central cylindrical portion in the micelle. The parameter $\hat{\varepsilon}$ is the depth of the attractive potential between cylindrical micelles. It should be noted that the aggregation number N is essentially governed by multiple equilibria among the micelles with various N and by the intermicellar interactions to some extent.[32] The parameters g_2 and $\hat{\varepsilon}$ play dominant role in the former and in the latter, respectively. We refer the expressions for the functions $M_w(c)$ and $A(c)$ to the original papers (ref 5 and 6) and our previous papers,[1,3] since they are fairly involved.

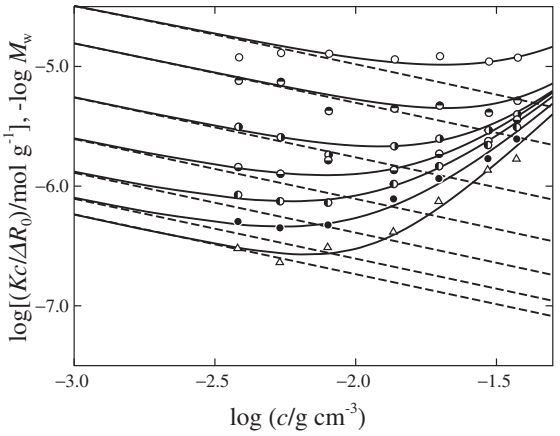

Figure 6. The results of the curve fitting for the plots of $Kc/\Delta R_0$ against c for the $C_{14}E_7$ micelle solutions at various T: Symbols have the same meaning as those in Figure 2c. The solid and dashed curves represent the calculated values of $Kc/\Delta R_0$ and $1/M_w(c)$, respectively. Temperatures T are 25.0, 30.0, 35.0, 40.0, 45.0, 50.0, and 55.0 °C from top to bottom, respectively.

Figures 4, 5, and 6 demonstrate the results of curve-fitting of the theoretical calculations to the experimental values of $Kc/\Delta R_0$ for the $C_{12}E_5$, $C_{12}E_7$, and $C_{14}E_7$ micelle solutions, respectively. In practice, we have calculated the theoretical values of $Kc/\Delta R_0$ as a function of c for various sets of the values of d, g_2, and $\hat{\varepsilon}$, and chosen the best-fit one to the observed results at fixed T for respective micelle solutions, thereby obtaining the $M_w(c)$ values at finite concentrations at each T. The solid curves in the figures represent the

best-fit theoretical curves thus determined. It is seen that they are in good coincidence with the respective data points at given temperatures. The good agreement implies that the $C_{12}E_5$, $C_{12}E_7$, and $C_{14}E_7$ micelles in dilute aqueous solutions may be represented by the wormlike spherocylinder model. The dashed lines represent the values of $1/M_w(c)$ at respective temperatures. For all the micelles at any fixed T, they are straight lines with a slope of -0.5, showing that M_w increases with c following a relation $M_w \propto c^{1/2}$ in the range of c examined, as in the case of the previous findings for the $C_{12}E_6$ and $C_{14}E_6$ micelles,[1] for the $C_{14}E_8$, $C_{16}E_8$ and $C_{18}E_8$ micelles,[2] for the $C_{10}E_5$ and $C_{12}E_5$ micelles,[3] and for the $C_{16}E_7$ and $C_{18}E_7$ micelles.[4] These results are in good correspondence with simple theoretical predictions derived from the thermodynamic treatments of multiple equilibria among micelles of various aggregation numbers.[5,30–32] The solid and dashed curves coincide with each other at small c and the difference between them steadily increases with increasing c. The results indicate that contributions of the virial coefficient terms, that is, the second term of the right hand side of eq 13, to $Kc/\Delta R_0$ are negligible at small c but progressively increase with increasing c as expected.

The d values obtained for the $C_{12}E_5$, $C_{12}E_7$, and $C_{14}E_7$ micelles are 2.2, 2.4, and 2.4 nm, respectively, at any T examined. The values of g_2 and $\hat{\varepsilon}$ determined are plotted against T in Figures 7 and 8, respectively. For each micelle, g_2 is an increasing function of T. On the other hand, $\hat{\varepsilon}$ does not show clear systematic dependence on the surfactant species, but is roughly constant $\hat{\varepsilon}/k_BT \simeq 3.3 \pm 0.3$ except for the one point at the lowest T for the $C_{14}E_7$ micelle solutions. It is found that when compared at fixed T, the g_2 value is larger for the $C_{14}E_7$ micelles than for the $C_{12}E_7$ micelles and that for the $C_{12}E_5$ micelles is larger than that for the $C_{12}E_7$ micelles. Thus, attractive (hydrophobic) interactions among C_iE_j molecules are considered to become stronger with increasing i if j is fixed and with decreasing j if i is fixed.

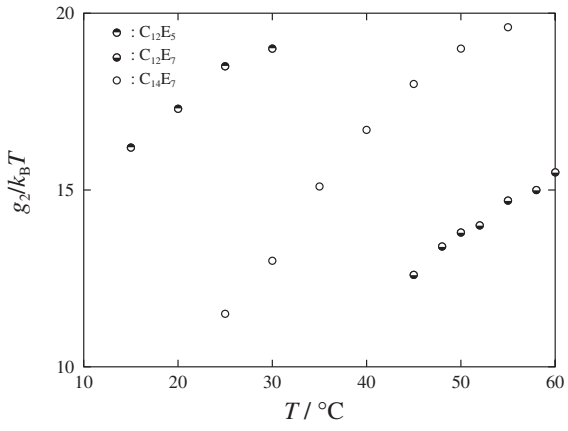

Figure 7. Temperature dependence of g_2 for the $C_{12}E_5$ + water (◓), $C_{12}E_7$ + water (○), and $C_{14}E_7$ + water (◒) systems.

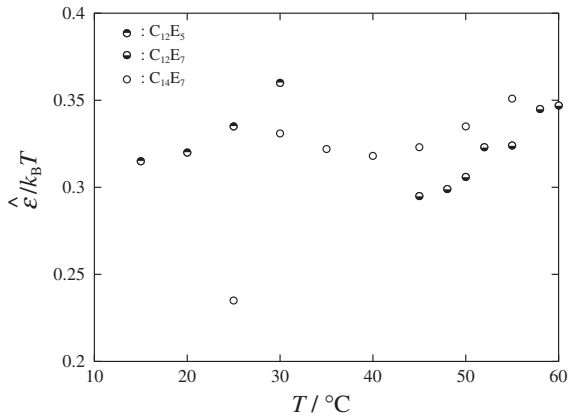

Figure 8. Temperature dependence of $\hat{\varepsilon}$ for the $C_{12}E_5$ + water (◓), $C_{12}E_7$ + water (○), and $C_{14}E_7$ + water (◒) systems.

Molar Mass Dependence of Radius of Gyration

The values of $\langle S^2\rangle_{app}^{1/2}$ determined at various T and c by eq 2 for the $C_{12}E_5$, $C_{12}E_7$, and $C_{14}E_7$ micelles are summarized in Tables I, II, and III, respectively, along with those of M_w. They are double-logarithmically plotted against M_w in Figures 9a, 9b, and 9c, respectively. For each of the micelles, the data points at various T and c are found to form a single composite curve, although they are rather scattered, suggesting that the values of $\langle S^2\rangle_{app}^{1/2}$ determined at finite c correspond to those of $\langle S^2\rangle^{1/2}$ for the individual micelles free from inter- and intra-micellar interactions or excluded volume effects. Thus, we have analyzed them by using the equation for the wormlike chain model written as[7]

$$\lambda^2\langle S^2\rangle = \frac{\lambda L}{6} - \frac{1}{4} + \frac{1}{4\lambda L} - \frac{1}{8\lambda^2 L^2}(1 - e^{-2\lambda L}) \quad (14)$$

along with the relation

$$L_w = \frac{4\nu M_w}{\pi N_A d^2} + \frac{d}{3} \quad (15)$$

Here, the relation between L_w and M_w is derived from the micellar volume and L_w is used in place of L in eq 14.

The solid curves in Figure 9 show the best-fit theoretical values of $\langle S^2\rangle^{1/2}$ for each micelle. Here, we have used the values of d determined above from the analyses of the SLS data and then evaluated λ^{-1} as 25.0, 25.0, and 20.0 nm for the $C_{12}E_5$, $C_{12}E_7$, and $C_{14}E_7$ micelles, respectively. It is found that the calculated results well explains the observed behavior of $\langle S^2\rangle_{app}^{1/2}$. This agreement again shows that the $C_{12}E_5$, $C_{12}E_7$, and $C_{14}E_7$ micelles assume a shape of wormlike spherocylinder.

Table I. Values of M_w, $\langle S^2\rangle_{app}^{1/2}$, and $R_{H,app}$ for $C_{12}E_5$ micelles at various T and c

$10^2c/g\,cm^{-3}$	$10^{-4}M_w$	$\langle S^2\rangle_{app}^{1/2}$/nm	$R_{H,app}$/nm
	$T = 15.0\,^\circ C$		
0.2686	39.9		
0.3936	48.3	12.0	12.8
0.4696	52.8	36.8	11.7
0.8009	69.0	42.0	15.2
1.4826	94.0	47.6	34.2
1.5537	96.2	15.9	33.8
2.2396	116	52.4	40.3
2.9423	133	70.2	57.3
4.9236	173	97.9	105
	$T = 20.0\,^\circ C$		
0.2684	69.2		
0.3932	83.7	20.8	18.3
0.4692	91.5	42.0	15.7
0.8001	120	52.9	28.4
1.4813	163	47.8	59.4
1.5523	167	25.9	52.0
2.2376	200	64.2	67.6
2.9396	230	90.0	98.3
4.9192	299	110	182
	$T = 25.0\,^\circ C$		
0.2681	126		
0.3928	152	37.1	25.3
0.4687	167	53.2	25.6
0.7992	218	67.1	35.3
1.4796	296	87.7	61.3
1.5505	303	50.7	83.6
2.2350	364	85.7	115
2.9362	418	112	138
4.9135	542	133	319
	$T = 30.0\,^\circ C$		
0.2677	197		
0.3922	239	18.7	25.8
0.4680	261	60.7	25.7
0.7981	341	74.2	32.2
1.4775	463	102	73.3
1.5484	474	76.3	86.5
2.2319	570	96.0	139
2.9321	653	121	159
4.9066	846	163	524

Hydrodynamic Radius of the Micelles

The values of $R_{H,app}$ determined by eq 10 at various T and c for $C_{12}E_5$, $C_{12}E_7$, and $C_{14}E_7$ micelles are summarized in Tables I, II, and III, respectively, along with those of M_w and $\langle S^2\rangle^{1/2}$. It is found that at any given T, $R_{H,app}$ increases with increasing c. The increase of $R_{H,app}$ reflects two effects; micellar growth in size and enhancement of the effects of the intermicellar hydrodynamic interactions with increasing c. The $R_{H,app}$ values, therefore, do not necessarily correspond to those for "isolated" micelles.

In Figures 10, 11, and 12 are shown double-logarithmic plots of $R_{H,app}$ against M_w for the $C_{12}E_5$, $C_{12}E_7$,

Table II. Values of M_w, $\langle S^2\rangle_{app}^{1/2}$, and $R_{H,app}$ for $C_{12}E_7$ micelles at various T and c

$10^2c/g\,cm^{-3}$	$10^{-4}M_w$	$\langle S^2\rangle_{app}^{1/2}$/nm	$R_{H,app}$/nm
	$T = 45.0\,^\circ C$		
0.3032	8.86	28.3	
0.5906	12.4	29.3	9.66
0.7883	14.3	17.2	9.26
0.8950	15.2	18.6	6.11
1.2124	17.7	20.8	7.99
1.5174	19.8	18.9	7.36
2.4793	25.4	26.9	11.0
2.9773	27.8	26.8	11.4
4.0169	32.4	12.5	17.9
4.9912	36.3	13.8	22.0
5.9317	39.7	33.0	28.0
6.9349	43.0	38.0	33.2
	$T = 48.0\,^\circ C$		
0.3028	13.2	21.7	
0.5898	18.4	23.1	7.48
0.7873	21.2	16.2	9.15
0.8939	22.6	21.8	8.39
1.2108	26.4	19.0	9.28
1.5155	29.5	22.0	10.3
2.4761	37.8	25.3	15.4
2.9734	41.5	29.6	14.5
4.0117	48.3	24.0	25.0
4.9848	54.0	25.7	32.4
5.9241	59.1	19.1	41.6
6.9259	64.1	42.5	52.0
	$T = 50.0\,^\circ C$		
0.3025	16.1	24.9	
0.5893	22.4	23.5	8.21
0.7866	25.9	17.6	12.7
0.8931	27.6	22.0	8.58
1.2097	32.2	16.2	8.57
1.5141	36.0	25.5	12.1
2.4738	46.1	27.6	18.5
2.9707	50.6	33.2	19.8
4.0081	58.9	18.9	31.6
4.9803	65.8	22.5	41.1
5.9187	72.0	44.1	48.0
6.9197	78.0	43.2	60.7
	$T = 52.0\,^\circ C$		
0.3022	17.7	20.0	
0.5887	24.8	21.7	8.71
0.7859	28.6	21.1	8.42
0.8923	30.5	23.8	11.3
1.2086	35.5	15.6	11.7
1.5127	39.7	28.2	13.0
2.4716	50.8	29.4	18.6
2.9681	55.7	34.8	19.3
4.0045	64.9	16.8	35.0
4.9758	72.4	18.9	41.4
5.9135	79.1	41.7	49.2
6.9135	85.8	45.3	62.0

Continued.

Continued.

$10^2 c/\mathrm{g\,cm^{-3}}$	$10^{-4}M_w$	$\langle S^2\rangle_{app}^{1/2}$/nm	$R_{H,app}$/nm
	$T = 55.0\,^\circ$C		
0.3018	25.1	21.4	
0.5879	35.1	22.8	8.36
0.7847	40.5	20.4	12.2
0.8910	43.2	20.5	12.0
1.2068	50.3	17.4	11.6
1.5105	56.3	25.4	13.9
2.4680	72.1	31.6	25.7
2.9637	79.0	35.4	28.8
3.9986	91.9	27.1	47.0
4.9684	103	29.1	59.6
5.9046	112	49.1	74.2
6.9032	122	58.8	93.6
	$T = 58.0\,^\circ$C		
0.3014	29.2	22.0	
0.5870	40.7	23.2	11.0
0.7835	47.0	23.1	12.0
0.8897	50.1	26.0	25.0
1.2051	58.3	21.3	14.5
1.5083	65.3	30.5	16.6
2.4644	83.4	27.7	10.7
2.9594	91.5	38.0	34.2
3.9928	106	25.7	43.8
4.9612	118	28.8	57.2
5.8961	130	52.8	81.5
6.8932	140	49.8	102
	$T = 60.0\,^\circ$C		
0.3010	37.4	21.7	
0.5864	52.2	23.7	11.1
0.7827	60.3	26.9	15.6
0.8887	64.3	27.7	16.7
1.2038	74.8	24.4	16.5
1.5067	83.7	29.9	20.7
2.4617	107	42.1	42.3
2.9562	117	41.6	37.6
3.9885	136	23.5	62.5
4.9559	152	29.1	85.9
5.8897	166	58.1	115
6.8858	180	60.0	138

and $C_{14}E_7$ micelles, respectively. As M_w is decreased, *i.e.*, c is lowered, $R_{H,app}$ at fixed T decreases following the curve convex downward shown by the dashed line. In our previous papers,[1–3] it has been indicated that in similar plots, the data points at different T asymptotically form a single composite curve at low c, or small M_w, implying that the effects of the intermicellar hydrodynamic interactions on $R_{H,app}$ become less significant as c is lowered and are negligible in the asymptotic region of low c. The present results are similar to the previous findings. We, therefore, analyze the data points at small M_w at each fixed T in Figures 10, 11, and 12 by regarding them to provide the relationship between R_H and M_w for "isolated" micelles without the intermicellar hydrodynamic interaction.

Table III. Values of M_w, $\langle S^2\rangle_{app}^{1/2}$, and $R_{H,app}$ for $C_{14}E_7$ micelles at various T and c

$10^2 c/\mathrm{g\,cm^{-3}}$	$10^{-4}M_w$	$\langle S^2\rangle_{app}^{1/2}$/nm	$R_{H,app}$/nm
	$T = 25.0\,^\circ$C		
0.3852	5.97	24.8	
0.5436	7.07	17.0	6.1
0.8042	8.59	17.6	6.4
1.3764	11.3	17.9	7.9
1.9927	13.6	26.2	9.4
2.9766	16.7	14.5	8.9
3.8159	19.0	26.9	11.4
	$T = 30.0\,^\circ$C		
0.3845	12.5	30.2	9.6
0.5426	14.8	17.0	11.8
0.8027	18.0	13.7	5.9
1.3737	23.6	18.0	11.4
1.9888	28.4	25.8	12.3
2.9708	34.7	14.8	11.8
3.8085	39.4	24.4	15.8
	$T = 35.0\,^\circ$C		
0.3837	33.8	24.7	14.1
0.5415	40.2	17.3	14.4
0.8011	48.9	23.9	10.4
1.3711	64.0	24.9	15.6
1.9850	77.1	28.2	24.3
2.9650	94.4	39.1	30.8
3.8011	107	36.1	44.4
	$T = 40.0\,^\circ$C		
0.3830	79.1	31.4	12.7
0.5405	94.0	31.1	21.5
0.7996	114	36.1	18.9
1.3684	150	40.4	32.4
1.9811	180	44.2	48.3
2.9593	221	57.2	66.2
3.7938	250	65.5	107
	$T = 45.0\,^\circ$C		
0.3822	151	40.9	26.1
0.5394	180	42.5	24.6
0.7980	219	53.6	32.4
1.3658	286	50.2	58.8
1.9773	345	64.8	85.4
2.9536	422	74.6	129
3.7865	479	87.0	200
	$T = 50.0\,^\circ$C		
0.3815	249	52.9	30.8
0.5384	296	57.0	37.6
0.7965	360	63.1	41.3
1.3631	471	69.3	88.5
1.9735	568	80.7	140
2.9479	694	95.3	195
3.7792	787	94.7	319
	$T = 55.0\,^\circ$C		
0.3808	336	58.9	30.2
0.5374	399	65.9	33.0
0.7949	485	77.8	50.3
1.3605	635	82.7	103
1.9697	764	96.3	146
2.9422	934	117	268
3.7719	1060	134	91.4

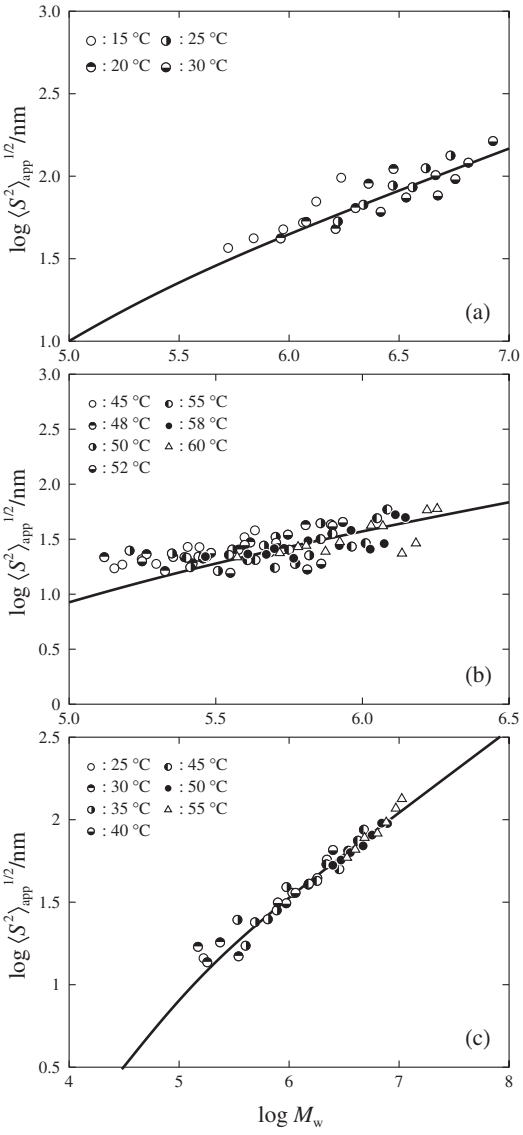

Figure 9. Double-logarithmic plots of $\langle S^2\rangle_{app}^{1/2}$ against M_w for the $C_{12}E_5$ (a), $C_{12}E_7$ (b), and $C_{14}E_7$ (c) micelles. Various symbols have the same meaning as those in Figure 2. The solid curve represents the theoretical values calculated by eqs 14 and 15.

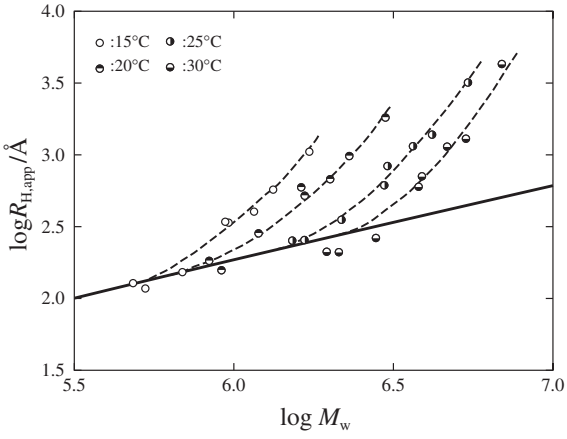

Figure 10. Double-logarithmic plots of $R_{H,app}$ against M_w for all the $C_{12}E_5$ micelle solutions: Various symbols have the same meaning as those in Figure 3a. The dashed curves are drawn to guide the eye. The solid curve represents the theoretical values calculated by eqs 15 and 16.

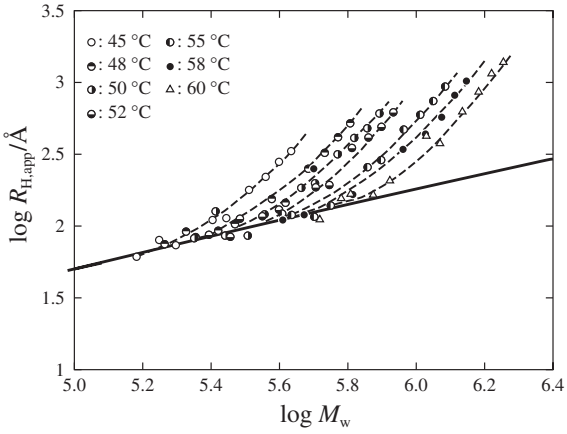

Figure 11. Double-logarithmic plots of $R_{H,app}$ against M_w for all the $C_{12}E_7$ micelle solutions: Various symbols have the same meaning as those in Figure 3b. The dashed curves are drawn to guide the eye. The solid curve represents the theoretical values calculated by eqs 15 and 16.

The translational diffusion coefficient D_0 of an isolated molecule is formulated by Norisuye *et al.*[8] for the wormlike spherocylinder model near the rod limit and by Yamakawa *et al.*[9,10] for the wormlike cylinder model, as a function of L with including the parameters d and λ^{-1}. Combining these theoretical results, we can calculate R_H as a function of L, d, and λ^{-1} over the entire range of L including the sphere, *i.e.*, the case $L = d$. The equation for R_H reads

$$R_H = \frac{L}{2f(\lambda L, \lambda d)} \qquad (16)$$

The expression for the function f is so lengthy that we refer it to the original papers.[8–10] By eqs 15 and 16, the theoretical values of R_H have been calculated as a function of M_w for various values of λ^{-1} with the use of the d values 2.2, 2.4, and 2.4 nm determined above for the $C_{12}E_5$, $C_{12}E_7$, and $C_{14}E_7$ micelles, respectively. Here, L in eq 16 is replaced by L_w given by eq 15. In Figures 10, 11, and 12, the solid lines represent best-fit curves to the data points for which the effects of the intermicellar hydrodynamic interactions are considered to be negligible. It is found that the theoretical curves well describe the observed behavior of R_H as a function of M_w, implying that the micelles may be represented with the wormlike spherocylinder model. We note that the data points at two lowest T in Figure 12 deviate upward from the theoretical curve even at lowest c for the reason unknown at present. The data points at fixed T steeply increase with M_w deviating upward from the solid

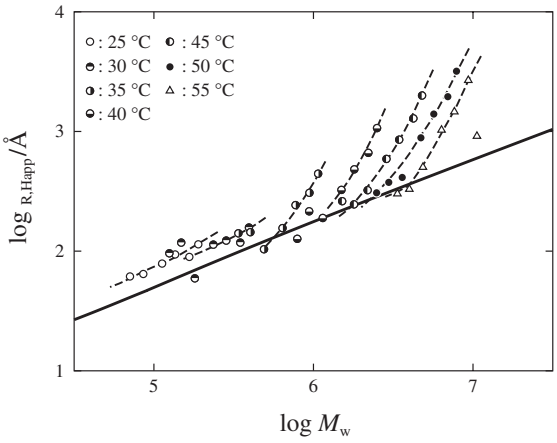

Figure 12. Double-logarithmic plots of $R_{H,app}$ against M_w for all the $C_{14}E_7$ micelle solutions: Various symbols have the same meaning as those in Figure 3c. The dashed curves are drawn to guide the eye. The solid curve represents the theoretical values calculated by eqs 15 and 16.

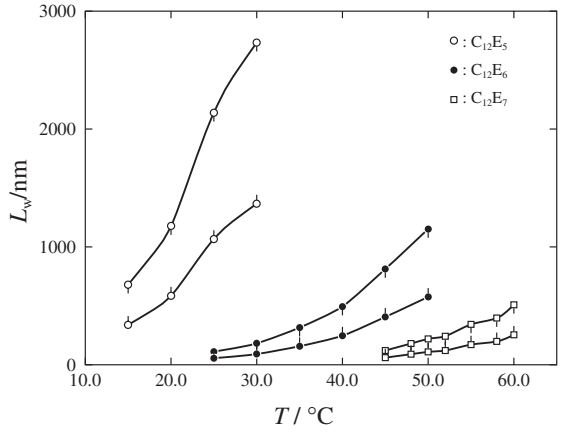

Figure 13. Temperature dependence of L for the $C_{12}E_5$ (○), $C_{12}E_6$ (●),[1] and $C_{12}E_7$ (□) micelles at $c = 0.01$ (pip up) and 0.04 (pip down) g/cm^3.

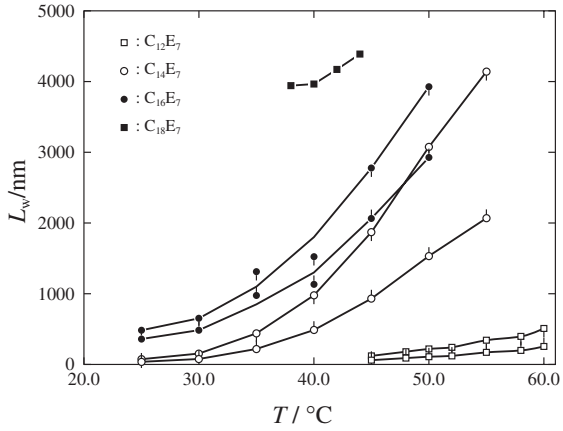

Figure 14. Temperature dependence of L for the $C_{12}E_7$ (□), $C_{14}E_7$ (○), $C_{16}E_7$ (●)[4] micelles at $c = 0.01$ (pip up) and 0.04 (pip down) g/cm^3, and $C_{18}E_7$ (■)[4] micelles at $c = 0.002$ g/cm^3.

curve due to the enhancement of the intermicellar hydrodynamic interactions with increasing c.

From the curve fittings, we have obtained 12.0, 14.0, and 13.0 nm for the λ^{-1} values of the $C_{12}E_5$, $C_{12}E_7$, and $C_{14}E_7$ micelles. These values indicate that the micelles are far from rigid rod but considerably stiff compared with typical flexible polymers.[34] The λ^{-1} values are significantly smaller than those obtained above from the analyses of $\langle S^2 \rangle$. This difference may be attributed to the fact that there is a distribution in micellar size and different averages are reflected in $\langle S^2 \rangle_{app}^{1/2}$ and R_H. Sato[5] and Zoeller *et al.*[32] have theoretically shown that micelles with sufficiently large aggregation number N have the most probable distribution and the distribution affords a value *ca.* 2 as the ratio of the weight-average aggregation number N_w to the number-average N_n without regard to the existence of the inter- and intra-micellar thermodynamic or excluded-volume interactions. They have also showed that in the limit of extensive micellar growth, the relation $M_w \propto c^{1/2}$ is set up, as observed in Figures 4, 5, and 6 in the present case. It is, thus, anticipated that the micelles observed in this study are grown up to the degree long enough to realize the most probable distribution in size and the distribution affects the evaluation of λ^{-1} from $\langle S^2 \rangle^{1/2}$ and R_H.

Length of the Micelles

The weight-average micellar length L_w have been calculated by eq 15 from the values of $M_w(c)$ and d obtained above from the analyses of the SLS data, for the $C_{12}E_5$, $C_{12}E_7$, and $C_{14}E_7$ micelles at various T and at two concentrations $c = 0.01$ and 0.04 g/cm^3. The results are plotted against T in Figures 13 and 14, where the previous results for the $C_{12}E_6$ and $C_{16}E_7$ micelles at the same concentrations and for the $C_{18}E_7$ micelles at $c = 0.002$ g/cm^3 are included for comparison. For all the micelles, L becomes larger as T is raised. We note that the highest temperature examined for each micelle is close to respective LCST. The results are in correspondence to the fact that g_2 increases with raising temperature as shown in Figure 7.

In Figure 13, it is seen that the length L of the micelles $C_{12}E_j$ becomes shorter with increasing oxyethylene chain length j. This finding may be interpreted as follows. Since water is a good solvent for polyoxyethylene, the oxyethylene group of the surfactant C_iE_j molecule opt to join the surrounding water molecules, which stabilizes the micelle in water. The affinity among the oxyethylene groups and water molecules causes repulsive force between the adjacent oxyethylene chains on the surface of the micelle, for the one end of the chain is fixed to the micelle core. The repulsive force is considered to be stronger for longer the oxyethylene group and it works to make

more surface area of the micelle. This may be the reason why the $C_{12}E_j$ molecules form shorter micelles with increasing j.

As found in Figure 14, the C_iE_7 micelles grow to a greater length as longer the alkyl chain length i of the surfactant molecules. In this case, the number of the oxyethylene units in the hydrophilic group is fixed to 7 and then the strength in the repulsive force between the adjacent oxyethylene chains may remain constant for different C_iE_7 micelles. On the other hand, attractive force among alkyl chains of the surfactant molecules due to the hydrophobic interactions is considered to become stronger as i is increased. The effects may facilitate the growth of micelles to the greater length for the surfactant C_iE_7 with longer alkyl chain.

Characteristics of the Micelles: Dependence on the Hydrophobic and Hydrophilic Chain Length

The values of d, λ^{-1}, and the spacing s between the hydrophilic tails of adjacent surfactant molecules on the micellar surface are summarized in Tables IV, V, and VI, respectively, for the C_iE_j micelles studied in the present and previous work.[1–4] Here, s is evaluated from the values of d, L, and the aggregation number N_w calculated from M_w. In the Tables, the column and row represent the alkyl and oxyethylene chain lengths, respectively.

In Table IV, we find that the d value does not significantly vary with hydrophobic and hydrophilic chain length. The results imply that the alkyl and oxyethylene groups of C_iE_j molecules do not take a fully extended or *trans* zig-zag form but assume a randomly coiled form in the micelles, as mentioned in the previous papers.[1–3] Table V shows that λ^{-1} decreases with increasing alkyl chain length i at fixed j except for the C_iE_8 micelles and increases with j at fixed i. This suggests that the relative strength of the repulsive force due to the hydrophilic interaction among C_iE_j molecules in the micelle to the attractive force due to the hydrophobic interactions controls the stiffness parameter; the repulsive force between the adjacent oxyethylene chains contribute to make the micelles stiffer and the attractive force between the adjacent alkyl chains reduce stiffness.

In Table VI, it is found that the values of the spacing s become larger as the lengths of the alkyl and oxyethylene chains increase, except for the $C_{18}E_8$ micelle. According to the rotational isomeric state (RIS) model calculations by Flory,[35] root mean-square end-to-end distance $\langle R^2 \rangle^{1/2}$ of penta-, hexa-, hepta-, and octa-oxyethylene is 1.00, 1.12, 1.22, and 1.33 nm, respectively. The s values in Table VI roughly correspond to these values; at least, the RIS calculations explain the increase of s with increasing j. The approximate coincidence may suggest that the octaoxyethylene chains take a randomly coiled form and are moving by taking a random orientation in water.

Table IV. Values of the cross-sectional diameter d/nm

	E_5	E_6	E_7	E_8
C_{10}	2.6	2.6		
C_{12}	2.2	2.3	2.4	
C_{14}		2.4	2.4	2.3
C_{16}			2.5	2.4
C_{18}			2.5	3.2

Table V. Values of the stiffness parameter λ^{-1}/nm

	E_5	E_6	E_7	E_8
C_{10}	35.0	75.0		
C_{12}	12.0	14.0	14.0	
C_{14}		7.0	13.0	18.0
C_{16}			6.0	24.0
C_{18}			6.0	25.0

Table VI. Values of the spacing s/nm

	E_5	E_6	E_7	E_8
C_{10}	1.12	1.15		
C_{12}	1.25	1.29	1.33	
C_{14}		1.30	1.38	1.46
C_{16}			1.37	1.46
C_{18}			1.41	1.29

CONCLUSIONS

In the present work, we have studied the $C_{12}E_5$, $C_{12}E_7$, and $C_{14}E_7$ micelles by static (SLS) and dynamic light scattering (DLS) experiments by employing the same technique as used in the previous studies.[1–4] The results of $Kc/\Delta R_0$ from SLS have been analyzed with the aid of the thermodynamic theory[5] for light scattering of micelle solutions formulated with wormlike spherocylinder model, thereby yielding the molar mass $M_w(c)$ as a function of c along with the cross-sectional diameter d of the micelle. The good agreement between the calculated and observed $Kc/\Delta R_0$ as a function of c indicates that the micelles examined assume a shape of flexible spherocylinders in dilute solutions. It is also found that the mean-square radius of gyration $\langle S^2 \rangle$ and the hydrodynamic radius R_H of the individual "isolated" micelles as functions of M_w have been well described by the theories for the wormlike chain and the wormlike spherocylinder models, respectively.

From the analyses of the SLS and DLS results, we have evaluated micellar length L as a function of surfactant concentration c and temperature T, d, the stiffness parameter λ^{-1}, and the spacing s between the

adjacent hydrophilic tails of surfactant molecules on the micellar surface. Combining the present and previous[1–4] results for these quantities, we have examined effects of the hydrophobic (alkyl) i and hydrophilic (oxyethylene) chain length j on the characteristics of C_iE_j micelles. Salient features found are summarized as follows: (i) The micelles grow in length to a greater extent for larger i and smaller j, reflecting that among surfactant molecules, attractive force due to the hydrophobic interactions becomes stronger for larger i and repulsive force due to the hydrophilic interactions becomes weaker for smaller j. (ii) The d value does not significantly vary with the values of i and j, indicating that the alkyl and oxyethylene chains of the surfactant molecule assume a random-coil form. (iii) The stiffness parameter λ^{-1} decreases with increasing i at fixed j and increases with increasing j at fixed i, suggesting that the stiffness of the micelle is controlled by the relative strength of the repulsive force to the attractive one among the surfactant molecules. (iv) The spacing s increases with increasing i and j. The s values are roughly comparable to those of the end-to-end distance $\langle R^2 \rangle^{1/2}$ of oxyethylene chains evaluated by Flory's RIS calculations,[35] indicating that the oxyethylene tails are moving by taking a random orientation on the micellar surface.

Acknowledgment. The authors are grateful to members of the NKO Academy for valuable discussions and comments. This research was supported in part by Nara Women's University Intramural Grant for Project Research.

REFERENCES

1. S. Yoshimura, S. Shirai, and Y. Einaga, *J. Phys. Chem. B*, **108**, 15477 (2004).
2. N. Hamada and Y. Einaga, *J. Phys. Chem. B*, **109**, 6990 (2005).
3. K. Imanishi and Y. Einaga, *J. Phys. Chem. B*, **109**, 7574 (2005).
4. Y. Einaga, A. Kusumoto, and A. Noda, *Polym. J.*, **37**, 368 (2005).
5. T. Sato, *Langmuir*, **20**, 1095 (2004).
6. R. Koyama and T. Sato, *Macromolecules*, **35**, 2235 (2002).
7. H. Benoit and P. Doty, *J. Phys. Chem.*, **57**, 958 (1953).
8. T. Norisuye, M. Motowoka, and H. Fujita, *Macromolecules*, **12**, 320 (1979).
9. H. Yamakawa and M. Fujii, *Macromolecules*, **6**, 407 (1973).
10. H. Yamakawa and T. Yoshizaki, *Macromolecules*, **12**, 32 (1979).
11. W. Brown, R. Johnson, P. Stilbs, and B. Lindman, *J. Phys. Chem.*, **87**, 4548 (1983).
12. W. Brown and R. Rymdén, *J. Phys. Chem.*, **91**, 3565 (1987).
13. W. Brown, Z. Pu, and R. Rymdén, *J. Phys. Chem.*, **92**, 6086 (1988).
14. T. Imae, *J. Phys. Chem.*, **92**, 5721 (1988).
15. W. Richtering, W. Burchard, and H. Finkelmann, *J. Phys. Chem.*, **92**, 6032 (1988).
16. T. Kato and T. Seimiya, *J. Phys. Chem.*, **90**, 1986 (1986).
17. T. Kato, S. Anzai, and T. Seimiya, *J. Phys. Chem.*, **94**, 7255 (1990).
18. T. R. Carale and D. Blankschtein, *J. Phys. Chem.*, **96**, 455 (1992).
19. T. M. Kole, C. J. Richards, and M. R. Fisch, *J. Phys. Chem.*, **98**, 4949 (1994).
20. H. Strunk, P. Lang, and G. H. Findenegg, *J. Phys. Chem.*, **98**, 11557 (1994).
21. P. Schurtenberger, C. Cavaco, F. Tiberg, and O. Regev, *Langmuir*, **12**, 2894 (1996).
22. G. Jerke, J. S. Pedersen, S. U. Egelhaaf, and P. Schurtenberger, *Langmuir*, **14**, 6013 (1998).
23. O. Glatter, G. Fritz, H. Lindner, J. Brunner-Papela, R. Mittelbach, R. Strey, and S. U. Egelhaaf, *Langmuir*, **16**, 8692 (2000).
24. A. Bernheim-Groswasser, E. Wachtel, and Y. Talmon, *Langmuir*, **16**, 4131 (2000).
25. E. R. Pike, R. M. Pomeroy, and J. M. Vaughan, *J. Chem. Phys.*, **62**, 3188 (1975).
26. Y. Einaga, T. Mitani, J. Hashizume, and H. Fujita, *Polym. J.*, **11**, 565 (1979).
27. B. Berne and R. Pecora, "Dynamic Light Scattering," J. Wiley, New York, 1976.
28. P. Stepánek, W. Brown, and S. Hvidt, *Macromolecules*, **29**, 8888 (1996).
29. G. Briganti, S. Puvvada, and D. Blankschtein, *J. Phys. Chem.*, **95**, 8989 (1991).
30. D. Blankschtein, G. M. Thurston, and G. B. Benedek, *J. Chem. Phys.*, **85**, 7268 (1986).
31. M. E. Cates and S. J. Candou, *J. Phys. Condens. Matter*, **2**, 6869 (1990).
32. N. Zoeller, L. Lue, and D. Blankschtein, *Langmuir*, **13**, 5258 (1997).
33. M. Kurata, "Thermodynamics of Polymer Solutions," translated from the Japanese by H. Fujita, Harwood Academic, Chur, 1982.
34. Y. Tamai, T. Konishi, Y. Einaga, M. Fujii, and H. Yamakawa, *Macromolecules*, **23**, 4067 (1990).
35. P. J. Flory, "Statistical Mechanics of Chain Molecules," John Wiley & Sons, New York, 1969.